Journal of Building Technology, 2024, Volume 6, Issue 2
DOI: 10.32629/jbt.v6i2.2552
ISSN Online: 2717-5103
ISSN Print: 2705-1390

Nonlinear Analysis of Plane Frames Using a Co-Rotating Timoshenko Beam Element

W.T. Matias Silva*, A.A. Cunha, M.P. Duque Gutiérrez

Department of Civil and Environmental Engineering, University of Brasília, 70910-900 Brasília, DF, Brazil.
*Corresponding author. Email address: taylor@unb.br

Abstract: The present work describes a co-rotating shear flexible beam element without shear locking and integrating Euler-Bernoulli's and Timoshenko's beam theories. The co-rotational kinematics is based on the separation of the motion in deformational and rigid body components. The deformation of the beam element is composed by three natural modes of deformation: the extension mode, the symmetric bending mode, and the anti-symmetric bending mode. The respective generalized stresses from these natural modes are self-balanced, allowing the achievement of a consistent tangent stiffness matrix. In this paper, it is detailed and deduced all the algebraic steps for the deduction of the elastic stiffness matrix, the geometric stiffness matrix, and the co-rotation stiffness matrix. Some examples are presented and the numerical results demonstrate that the beam element here presented is able to handle large rotations.

Key words: Bernoulli/Timoshenko beam element; corotational kinematic; deformation's natural modes

1. Introduction

The last two decades have witnessed a growing interest among the computational mechanics community in the application of the corotational formulation in the nonlinear analysis of less common structures used in high technology sectors such as aerospace, aviation and petroleum. The main idea of the corotational formulation is to decompose the motion of a solid into the sum of a rigid body motion and a deformational displacement. This formulation represents a specific instance of Lagrangian kinematics, which is employed to model the consequences of geometric nonlinearity in structural analysis through the finite element method. Thus, within this formulation, it is assumed that both translations and rotations of the rigid body may be large, but the deformations must be small. Consequently, there exists the opportunity to utilize linear finite elements in problems that involve geometric nonlinearity, which serves as the primary impetus for adopting the corotational formulation. In the 1970s and 1980s, this formulation was used in the nonlinear analysis of a class of structures employed in aerospace engineering (airplanes, satellites, rockets, antennas), in naval engineering (ships, offshore platforms), as well as in mechanical engineering (robotics, excavation machines), having little impact on civil engineering at that time. In the mid-1990s, the formulation was extended to the analysis of local failure models and applications encompassing nonlinear dynamics. In the work of Skallerud et al. [1], the corotational formulation is used to analyze subsea gas pipelines exposed to large geometric changes as well as local failures. Yaw et al. [2] show applications of the corotational formulation and meshless methods in the analysis of 2D solids, including geometric and physical nonlinearity. Felippa and Haugen [3] describe a unified corotational formulation for nonlinear static analysis of discretized

solids by means of beam, plate and sheet elements. In the work of Mostafa et al. [4], the formulation is extended for static analysis using 2D solid finite elements, 3D solids and so-called low-order solid-sheet elements with enhanced deformation fields, which have only a few translational degrees of freedom. On the other hand, Matias and Bezerra [5] proposed a unified formulation for the corotational description of 2D beam and spatial articulated structure elements. Finally, other authors [6, 7] who have applied the corotational formulation for nonlinear dynamic analysis of discretized structural systems with 2D and 3D beam elements can be cited. In this paper, the corotational formulation of a 2D beam element is presented with the following particularities: (a) a vector of rigid body displacements of the element is defined through a local reference frame fixed at its centroid; (b) this element can undergo rigid body rotation of any magnitude due to the application of the modulus function; (c) three natural deformation modes [8, 9] will be adopted to represent the deformational part of the element motion; d) these natural deformation modes represent self-equilibrated internal forces; e) the vector of nodal forces is obtained from the self-equilibrated internal forces; f) the principle of complementary virtual works [10, 11] is used to obtain the elastic stiffness matrix, integrating the Euler-Bernoulli and Timoshenko beam theories; g) this element will be referred to here as a unified 2D beam element; h) this element does not present shear locking; i) the algebraic development for the calculation of the corotational and geometric stiffness matrices is described in detail, along with the complete expression of the tangent stiffness matrix. Finally, this element is applied to the nonlinear analysis of plane frames. Numerical examples are presented in which the non-existence of shear blocking in the nonlinear analysis is verified.

2. Corotational Description

It is a global coordinate system based on orthogonality, as shown in Figure 1. To express the kinematic variables in the non-deformed configuration, the material coordinates (X, Y) are used, while in the deformed configuration the spatial coordinates (x, y) are used. In the non-deformed configuration, the nodal coordinates of the element are given by (X_1, Y_1) and (X_2, Y_2), respectively. Its initial length and inclination are given by:

$$\begin{aligned} l_0 &= \sqrt{X_{21}^2 + Y_{21}^2} \\ \varphi_0 &= 2\arctan\left(\frac{l_0 - X_{21}}{Y_{21}}\right) \end{aligned} \qquad (1)$$

Where $X_{21} = X_2 - X_1$ and $Y_{21} = Y_2 - Y_1$. To obtain the expression (1b), the relation $\tan(1/2\varphi_0)$ was used. This expression is singular if $Y_{21} = 0$, so the value of $\varphi_0 = 0$ is assigned for $X_{21} = l_0$ or $\varphi_0 = \pi$, for $X_{21} = -l_0$. Similarly, in the deformed configuration, the nodal coordinates of the element are given by (x_1, y_1) and (x_2, y_2), respectively. Its actual length and inclination are given by:

$$\begin{aligned} l &= \sqrt{x_{21}^2 + y_{21}^2} \\ \varphi &= 2\arctan\left(\frac{l - x_{21}}{y_{21}}\right) \end{aligned} \qquad (2)$$

Where $X_{21} = X_2 - X_1$ and $Y_{21} = Y_2 - Y_1$. Again, the relation $\tan(1/2\varphi_0)$ was used to obtain the expression (2b). This expression is singular if $y_{21} = 0$, where $\varphi = 0$ for $x_{21} = l$ or $\varphi = \pi$ for $x_{21} = -l$. As shown in Figure 1, the motion of the 2D beam element is given by the vector of nodal displacements in global coordinates as:

$$\boldsymbol{u}^T = (u_1, v_1, \theta_1, u_2, v_2, \theta_2) \qquad (3)$$

On the other hand, the nodal spatial coordinates can be written as a function of the nodal displacements as $x_1 = X_1 + u_1$ and $x_2 = X_2 + u_2$, respectively. From these expressions, we obtain that $x_{21} = X_{21} + u_{21}$ and $y_{21} = Y_{21} + u_{21}$, where $u_{21} = u_2 - u_1$ and $v_{21} = v_2 - v_1$, which allows us to rewrite that: $l = \sqrt{(X_{21} + u_{21})^2 + (Y_{21} + v_{21})^2}$

To define the rigid body motion of this element, a local coordinate system (x_e, y_e) is fixed at its centroid and accompanies it throughout its motion, as shown in Figure 1. Thus, the rigid body motion is defined by two translations and one rotation of the local reference frame between the deformed and undeformed configurations, and is written as:

$$\boldsymbol{u}_r = \begin{Bmatrix} \frac{1}{2}(u_2 + u_1) \\ \frac{1}{2}(v_2 + v_1) \\ \varphi - \varphi_0 \end{Bmatrix} \tag{4}$$

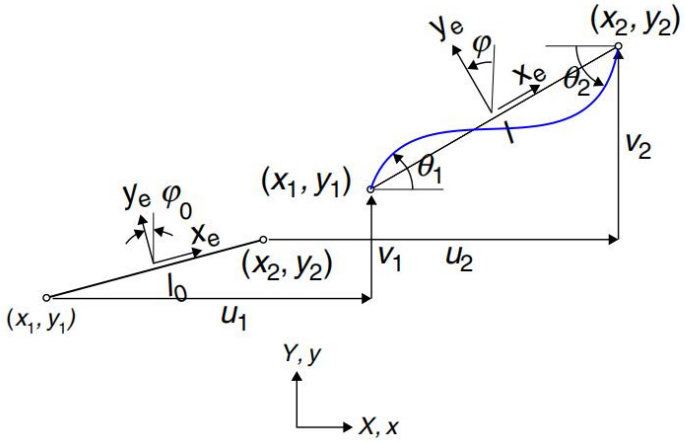

Figure 1. Movement of the 2D beam element.

2.1 Natural modes of deformation

Three degrees of freedom were necessary to define the rigid body motion of the 2D beam element, thus the remaining three degrees of freedom are necessary to define the deformational motion of the element. In this work, the concept of the natural modes of deformation defined in references [8, 9] is adopted. For the case of the 2D beam element, three natural deformation modes are defined as shown in Figure 2. The first mode is obtained by applying an axial tensile stress to the nodes of the element. The second mode is obtained by considering the element subjected to a state of pure bending which implies in the absence of shear stress. This mode defines a symmetric elastic line. In the third mode, the element is subjected to a state of simple bending resulting in constant shear stress. This mode defines an anti-symmetric elastic line. Therefore, the vector of deformational displacements with respect to the local coordinate system is defined as:

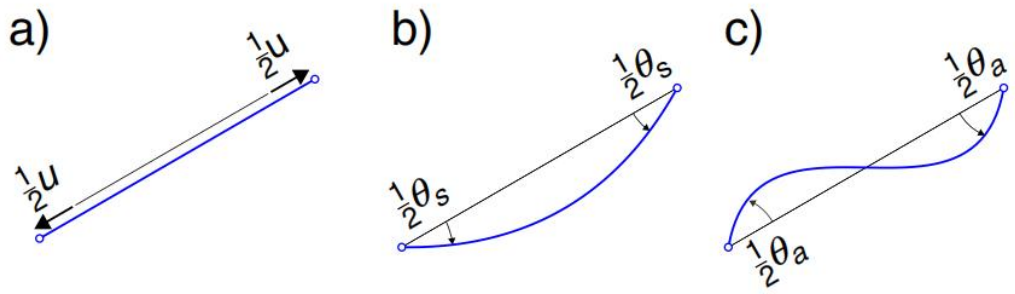

Figure 2. Natural modes of deformation. a) Stretching. b) Symmetric elastic. c) Anti-symmetric elastic.

$$\boldsymbol{u}_d^T = (u, \theta_s, \theta_a) \tag{5}$$

Where

$$\begin{aligned} u &= l - l_0 \\ \theta_s &= \theta_2 - \theta_1 \\ \theta_a &= \theta_2 + \theta_1 - 2(\varphi - \varphi_0) \end{aligned} \tag{6}$$

To obtain expressions (6b) and (6c), the deformation rotations of the element nodes are used, which are defined as θ_1 - (φ - φ_0) and θ_2 - (φ - φ_0), respectively, according to Figure 1. Then, according to Figs. 2b and 2c, the symmetric and anti-symmetric rotations of each element node are summed. Finally, these rotations are equated to the deformational rotations of the element nodes described in Figure 1. This procedure generates the following system of Equations:

$$\begin{aligned} -\frac{1}{2}\theta_s + \frac{1}{2}\theta_a &= \theta_1 - (\varphi - \varphi_0) \\ \frac{1}{2}\theta_s + \frac{1}{2}\theta_a &= \theta_2 - (\varphi - \varphi_0) \end{aligned} \tag{7}$$

Solving this system obtains the values of θs and θa described in Equations (6b) and (6c), respectively. In order to assume any magnitude in the value of the angles, the expression for anti-symmetric rotation must be calculated using the modulus function [11], such that:

$$\theta_a = \underset{2\pi}{\text{mod}}(\theta_a + \pi) - \pi \tag{8}$$

The modulus function places an arbitrary value in the interval [0, 2π], and the last term restores symmetry relative to the zero value. Omitting this step can lead to divergence problems when the 2D beam element undergoes rotations ±π, ± 2π, . . .

2.2 Vector of internal forces

It is important to note that the natural deformation modes generate self-equilibrated sectional stresses as shown in Figure 3. The natural deformation modes as well as their respective stresses are expressed in relation to the local reference frame. Therefore, the vector of self-equilibrated stresses is given by:

$$\boldsymbol{f}_d^T = (N, M_s, M_a) \tag{9}$$

The combination of the self-equilibrated sectional forces, shown in Figure 3, generates a vector of self-equilibrated nodal forces as shown in Figure 4c. The relationship of this vector to the vector of nodal forces in local coordinates, shown in Figure 4b, is given by the following expression:

$$\boldsymbol{f}^e = \boldsymbol{S}\boldsymbol{f}_d \tag{10}$$

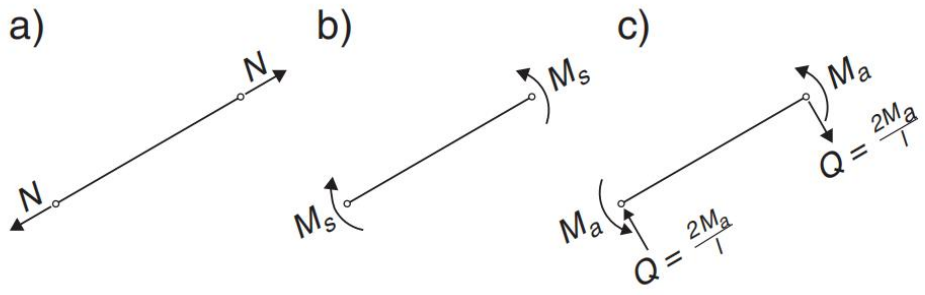

Figure 3. Self-balanced forces. a) Axial tensile force. b) Pure bending. c) Simple bending.

Where S is the transformation matrix given by:

$$\boldsymbol{S} = \begin{bmatrix} -1 & 0 & 0 \\ 0 & 0 & 2/l \\ 0 & -1 & 1 \\ 1 & 0 & 0 \\ 0 & 0 & -2/l \\ 0 & 1 & 1 \end{bmatrix} \tag{11}$$

Analogously, the relationship between the vector of nodal forces in local coordinates and the vector of nodal forces in global coordinates, shown in Figure 4a, is given by:

$$\boldsymbol{f} = \boldsymbol{R}\boldsymbol{f}^e \tag{12}$$

Where R is the rotation matrix of the local coordinate system for the global coordinate system given by:

$$\boldsymbol{R} = \begin{bmatrix} \cos\varphi & -\text{sen}\varphi & 0 & 0 & 0 & 0 \\ \text{sen}\varphi & \cos\varphi & 0 & 0 & 0 & 0 \\ 0 & 0 & 1 & 0 & 0 & 0 \\ 0 & 0 & 0 & \cos\varphi & -\text{sen}\varphi & 0 \\ 0 & 0 & 0 & \text{sen}\varphi & \cos\varphi & 0 \\ 0 & 0 & 0 & 0 & 0 & 1 \end{bmatrix} \tag{13}$$

Finally, substituting Equation (10) into (12), we obtain the relation between the vector of self-balanced forces and the vector of internal forces in global coordinates which is written as:

$$\boldsymbol{f} = \boldsymbol{R}\boldsymbol{S}\boldsymbol{f}_d \tag{14}$$

Note that the nodal displacements can be written relative to the local coordinate system as:

$$\boldsymbol{u}^e = \boldsymbol{R}^T\boldsymbol{u} \tag{15}$$

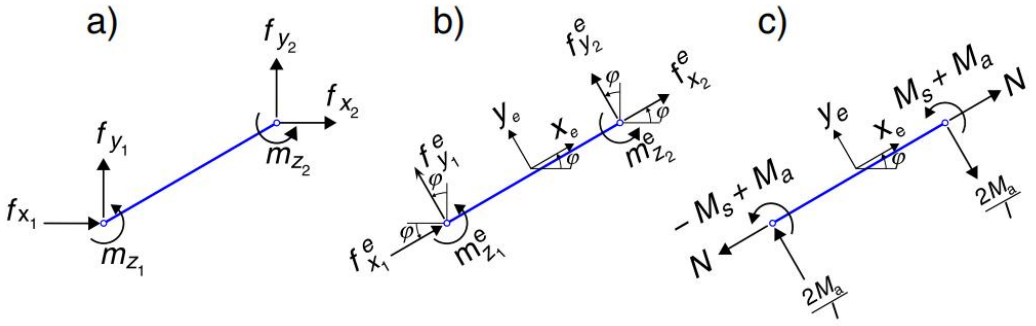

Figure 4. Nodal force vector. a) In global coordinates. b) In local coordinates. c) Self-balanced.

3. Obtaining the Tangent Stiffness Matrix

Based on the corotational kinematics, it is necessary to derive the expression of the tangent stiffness matrix in relation to the local reference frame fixed on the element. The tangent stiffness matrix expresses the relationship between the force increments and nodal displacements in local coordinates as:

$$d\boldsymbol{f}^e = \boldsymbol{K}^e d\boldsymbol{u}^e \tag{16}$$

Using Equations (12) and (15), the tangent stiffness matrix expressed in relation to the global coordinate system is obtained as follows:

$$\boldsymbol{K} = \boldsymbol{R}\boldsymbol{K}^{e}\boldsymbol{R}^{T} \tag{17}$$

Therefore, if the 2D beam element is considered in its current deformed configuration as shown in Figure 5, and an infinitesimal increment of displacement is applied from this equilibrium configuration, the variation of rigid body rotation and element length are written:

$$d\varphi = \frac{dv_2^e - dv_1^e}{l}, \quad dl = du_2^e - du_1^e \tag{18}$$

Where $du_1^e, dv_1^e, du_2^e, dv_2^e$ are the components of the increment of nodal displacements in relation to the local coordinate system. On the other hand, recalling that the internal work does not vary in relation to the different coordinate systems and taking into account Equation (10), the variation of the internal work can be written as:

$$dV = d\boldsymbol{u}^{e^T}\boldsymbol{f}^{e} = d\boldsymbol{u}^{e^T}\boldsymbol{S}\boldsymbol{f}_d = d\boldsymbol{u}_d^T\boldsymbol{f}_d \tag{19}$$

Where $d\boldsymbol{u}_d^T = (du, d\theta_s, d\theta_s)$ is the variation of the natural deformation modes. The last equality is satisfied for any arbitrary value of f_d, consequently it follows that:

$$d\boldsymbol{u}_d = \boldsymbol{S}^T d\boldsymbol{u}^{e} \tag{20}$$

The variation of the vector of internal forces given by Equation (14) is written as:

$$d\boldsymbol{f} = \boldsymbol{R}\boldsymbol{S}d\boldsymbol{f}_d + \boldsymbol{R}d\boldsymbol{S}\boldsymbol{f}_d + d\boldsymbol{R}\boldsymbol{S}\boldsymbol{f}_d \tag{21}$$

With

$$d\boldsymbol{R} = \begin{bmatrix} -\sin\varphi & -\cos\varphi & 0 & 0 & 0 & 0 \\ \cos\varphi & -\sin\varphi & 0 & 0 & 0 & 0 \\ 0 & 0 & 0 & 0 & 0 & 0 \\ 0 & 0 & 0 & -\sin\varphi & -\cos\varphi & 0 \\ 0 & 0 & 0 & \cos\varphi & -\sin\varphi & 0 \\ 0 & 0 & 0 & 0 & 0 & 0 \end{bmatrix} d\varphi,$$

$$d\boldsymbol{S} = \begin{bmatrix} 0 & 0 & 0 \\ 0 & 0 & -2/l^2 \\ 0 & 0 & 0 \\ 0 & 0 & 0 \\ 0 & 0 & 2/l^2 \\ 0 & 0 & 0 \end{bmatrix} dl \tag{22}$$

The relationship between the variations of the self-equilibrated sectional stresses and the natural deformation modes is given by:

$$d\boldsymbol{f}_d = \boldsymbol{K}_d d\boldsymbol{u}_d \tag{23}$$

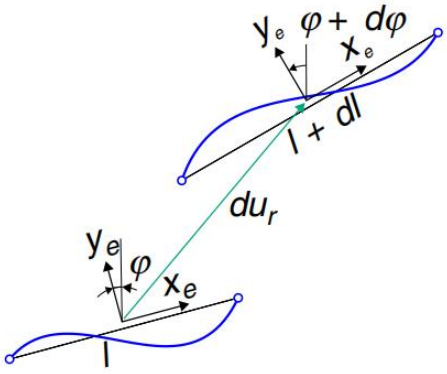

Figure 5. Incremental movement of the 2D beam element.

Where K_d is the elastic stiffness matrix of the element, whose dimension is 3 × 3. Taking into account the Equations (12), (20) and (23), the Equation (21) can be rewritten as:

$$d\boldsymbol{f}^e = \boldsymbol{S}\boldsymbol{K}_d\boldsymbol{S}^T\, d\boldsymbol{u}^e + (d\boldsymbol{S} + \boldsymbol{R}^T d\boldsymbol{R}\boldsymbol{S})\boldsymbol{f}_d \qquad (24)$$

Finally, taking into account Equation (16), the tangent stiffness matrix in relation to the local coordinate system can be written as:

$$\boldsymbol{K}^e = \boldsymbol{S}\boldsymbol{K}_d\boldsymbol{S}^T + \boldsymbol{K}_r \qquad (25)$$

Where the first term takes into account the stiffness coefficients of the natural deformation modes, while K_r is the corotational stiffness matrix, which represents the variation effect of the rigid body rotation of the local reference system and the effect of the shear stress due to the variation of the element length, which according to Equation (24), is defined as: $K_r = (\mathrm{dS} + \mathrm{R}^T\mathrm{dRS})f_d$. Note that according to Equation (22), the variation of the transformation matrix S depends on the variable dl and that the variation of the rotation matrix R depends on $d\varphi$. Considering Equations (18a) and (18b), after some algebraic developments one arrives at:

$$\boldsymbol{K}_r = \frac{1}{l}\begin{bmatrix} 0 & Q & 0 & 0 & -Q & 0 \\ Q & N & 0 & -Q & -N & 0 \\ 0 & 0 & 0 & 0 & 0 & 0 \\ 0 & -Q & 0 & 0 & Q & 0 \\ -Q & -N & 0 & Q & N & 0 \\ 0 & 0 & 0 & 0 & 0 & 0 \end{bmatrix} \qquad (26)$$

This matrix is part of the complete geometric stiffness matrix of the 2D beam element as will be demonstrated in section 3.3.

3.1 Elastic stiffness matrix

The first natural deformation mode is the elongation of the 2D beam element and its stiffness coefficient, according to the theory of strength of materials, is given by the incremental ratio $dN = EA/l \times du$. For the element in pure bending, the stiffness coefficient is obtained by applying the Principle of Complementary Virtual Work (CVWP) resulting in the following incremental relationship $dM_s = EI/l \times d\theta_s$. The third natural deformation mode represents the element subjected to simple bending resulting in a constant shear stress. Thus, when applying the CVWP, it is obtained that:

$$M_a\theta_a = \int_0^l \left(\frac{M(x)^2}{EI} + \frac{Q^2}{GA_0} \right) dx = \frac{1}{3}\frac{M_a^2 l}{EI} + \frac{Q^2 l}{GA_0} \tag{27}$$

Where A_0 is the cross-sectional area corrected by the shape factor that takes into account the effect of the shear stress distribution in the cross-section. The effect of shear deformation is introduced through the following parameters:

$$\psi_a = \frac{1}{1+\Phi}, \quad \Phi = \frac{12EI}{GA_0 l^2} \tag{28}$$

And using the shear stress expression $Q = 2M_a/l$ and Equation (27), the following incremental relationship is determined:

$$dM_a = 3\psi_a \frac{EI}{l} d\theta_a \tag{29}$$

Finally, the elastic stiffness matrix is defined as:

$$\boldsymbol{K}_d = \begin{bmatrix} \frac{EA}{l} & 0 & 0 \\ 0 & \frac{EI}{l} & 0 \\ 0 & 0 & 3\psi_a \frac{EI}{l} \end{bmatrix} \tag{30}$$

It should be noted that the bending stiffness coefficients of this matrix take into account both the Euler-Bernoulli hypothesis and the Timoshenko hypothesis, hence the name unified beam element.

3.2 Geometric stiffness matrix

In addition to the elastic stiffness matrix, it is necessary to take into account the geometric stiffness matrix due to the effect of axial stress when the 2D beam element undergoes a rigid body rotation increment. In this work, to obtain the coefficients of the geometric stiffness matrix, the differential Equation of the beam-column without transverse loads is considered and the shear effect is neglected. The simply supported beam element is considered, so that the boundary conditions of the second and third natural deformation modes are satisfied, as shown in Figures 2b and 2c. Thus, the differential governing Equation is written as:

$$EIv'''' - Nv'' = 0 \tag{31}$$

After applying the integration by parts twice, the following integral form of this Equation is obtained:

$$\int_0^l (\delta v'' EIv'' + \delta v' Nv')dx = [\delta v\, Q + \delta\theta M]_0^l \tag{32}$$

The incremental relationship of this integral form, after some algebraic steps, is expressed as:

$$\int_0^l (\delta v'' EI\, dv'' + \delta v' N dv')dx = [\delta v\, dQ + \delta\theta dM]_0^l \tag{33}$$

To calculate the geometric stiffness coefficient due to the second natural deformation mode, the following part of the integral form described above is applied:

$$\int_0^l \delta v' N dv' dx = [\delta\theta_s dM_s]_0^l \tag{34}$$

Both the incremental displacement field dυ and the virtual displacement field δυ, along with their first order derivatives, are interpolated using the shape function for the symmetric elastic defined in Figure 6. After applying the chain rule, we obtain that dυ' = 1/2ξdθ$_s$ and δυ' = 1/2ξdθ$_s$. Next, integrating Equation (34) in the coordinate space ξ, one arrives at:

$$dM_a = \frac{1}{12} N l d\theta_a \;\Rightarrow\; k_a = \frac{1}{20} N l \tag{35}$$

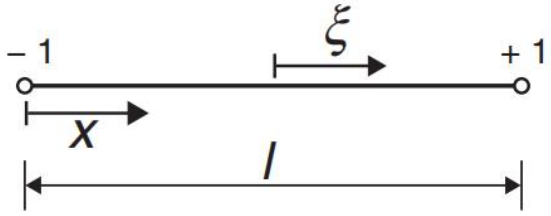

$$x = \frac{l}{2}(1+\xi) \qquad -1 \le \xi \le 1$$

$$\frac{dx}{d\xi} = \frac{l}{2} \Rightarrow \frac{d\xi}{dx} = \frac{2}{l}$$

Symmetrical elastic

Anti-symmetrical elastic

Chain rule

$$\frac{d(\cdot)}{dx} = \frac{d(\cdot)}{d\xi}\frac{d\xi}{dx}$$

Figure 6. Shape functions.

To calculate the geometric stiffness coefficient due to the third natural deformation mode, the following part of the integral form described in Equation (33) is applied:

$$\int_0^l \delta v' N dv' dx = [\delta\theta_a dM_a]_0^l \tag{36}$$

Following the previous steps and remembering that for the case of the anti-symmetric elastic when applying the chain rule we obtain that dυ' = -1/4(1-3ξ^2)dθ$_a$ and δυ' = -1/4(1-3ξ^2)dθ$_a$. Thus, integrating Equation (36) in the coordinate space ξ one arrives at:

$$dM_a = \frac{1}{12} N l d\theta_a \;\Rightarrow\; k_a = \frac{1}{20} N l \tag{37}$$

And the geometric stiffness matrix is defined as:

$$\boldsymbol{K}_g = \begin{bmatrix} 0 & 0 & 0 \\ 0 & \frac{1}{12} N l & 0 \\ 0 & 0 & \frac{1}{20} N l \end{bmatrix} \tag{38}$$

3.3 Full tangent stiffness matrix

To obtain the full tangent stiffness matrix of the 2D beam element, the matrices K_d and K_g are extended for their full forms, i.e., for 6 × 6 order matrices using the transformation matrix S. Consequently, the full form is written as:

$$\boldsymbol{K}^e = \boldsymbol{S}\boldsymbol{K}_d\boldsymbol{S}^T + \boldsymbol{S}\boldsymbol{K}_g\boldsymbol{S}^T + \boldsymbol{K}_r = \boldsymbol{K}_d^e + \boldsymbol{K}_g^e \tag{39}$$

With

$$\boldsymbol{K}_d^e = \begin{bmatrix} \frac{EA}{l} & 0 & 0 & -\frac{EA}{l} & 0 & 0 \\ 0 & 12\psi_a\frac{EI}{l^3} & 6\psi_a\frac{EI}{l^2} & 0 & -12\psi_a\frac{EI}{l^3} & 6\psi_a\frac{EI}{l^2} \\ 0 & 6\psi_a\frac{EI}{l^2} & (3\psi_a+1)\frac{EI}{l} & 0 & -6\psi_a\frac{EI}{l^2} & (3\psi_a-1)\frac{EI}{l} \\ -\frac{EA}{l} & 0 & 0 & \frac{EA}{l} & 0 & 0 \\ 0 & -12\psi_a\frac{EI}{l^3} & -6\psi_a\frac{EI}{l^2} & 0 & 12\psi_a\frac{EI}{l^3} & -6\psi_a\frac{EI}{l^2} \\ 0 & 6\psi_a\frac{EI}{l^2} & (3\psi_a-1)\frac{EI}{l} & 0 & -6\psi_a\frac{EI}{l^2} & (3\psi_a+1)\frac{EI}{l} \end{bmatrix} \quad (40)$$

$$\boldsymbol{K}_g^e = \boldsymbol{S}\boldsymbol{K}_g\boldsymbol{S}^T + \boldsymbol{K}_r = \frac{1}{l}\begin{bmatrix} 0 & Q & 0 & 0 & -Q & 0 \\ Q & \frac{6}{5}N & \frac{1}{10}Nl & -Q & -\frac{6}{5}N & \frac{1}{10}Nl \\ 0 & \frac{1}{10}Nl & \frac{2}{15}Nl^2 & 0 & -\frac{1}{10}Nl & -\frac{1}{30}Nl^2 \\ 0 & -Q & 0 & 0 & Q & 0 \\ -Q & -\frac{6}{5}N & -\frac{1}{10}Nl & Q & \frac{6}{5}N & -\frac{1}{10}Nl \\ 0 & \frac{1}{10}Nl & -\frac{1}{30}Nl^2 & 0 & -\frac{1}{10}Nl & \frac{2}{15}Nl^2 \end{bmatrix}$$

Where K^e is the tangent stiffness matrix, k_d^e is the material stiffness matrix and k_g^e is the geometric stiffness matrix of the 2D beam element. It should be noted that Turner et al. [12] were the first authors to obtain the material stiffness matrix for a Timoshenko beam element without shear locking. Przemieniecki [13], on the other hand, describes the material stiffness matrix as a function of the coefficient Φ, which is defined in (28), by solving an ordinary differential equation that takes into account the Timoshenko hypotheses. On the other hand, assuming $Q = 0$ in the geometric stiffness matrix in (40b), one arrives at the standard geometric stiffness matrix of the Euler-Bernoulli beam element which is described as

$$\boldsymbol{K}_g^e = \frac{N}{30l}\begin{bmatrix} 0 & 0 & 0 & 0 & 0 & 0 \\ 0 & 36 & 3l & 0 & -36 & 3l \\ 0 & 3l & 4l^2 & 0 & -3l & -l^2 \\ 0 & 0 & 0 & 0 & 0 & 0 \\ 0 & -36 & -3l & 0 & 36 & -3l \\ 0 & 3l & -l^2 & 0 & -3l & 4l^2 \end{bmatrix} \quad (41)$$

This matrix appears for the first time in the article published by Martin [14] in the 1960s.

4. Numerical Examples

To perform the geometric nonlinear analysis of the examples presented in this chapter, the authors of this paper used a Fortran90 program named co_rotating_2Dbeam.f90. Table 1 summarizes the main steps to be implemented in a computer program for the calculation of both the vector of internal forces and the tangent stiffness matrix of the 2D beam element expressed in global coordinates. In all the examples presented below, a convergence tolerance of 10^{-5} was adopted. The objective of this item is to show the performance of the unified beam element developed in this work to reproduce the strongly nonlinear behavior of some structural systems. It is important to highlight, as will be seen in the following examples, that the unified beam element described here does not present shear locking, besides its ability to deal with large rigid body rotations.

Table 1. Corrotational description algorithm

Displacement in global coordinates $\boldsymbol{u}^T = (u_1, v_1, \theta_1, u_2, v_2, \theta_2)$	(3)
Variable configuration $\boldsymbol{x}^T = \boldsymbol{X}^T + \boldsymbol{u}^T = (X_1 + u_1, Y_1 + v_1, \theta_1, u_2 + X_2, v_2 + Y_2, \theta_2)$	
Rigid body rotation: φ - φ0 $\varphi_0 = 2\arctan\left(\frac{l_0 - X_{21}}{Y_{21}}\right), \quad \varphi = 2\arctan\left(\frac{l - x_{21}}{y_{21}}\right)$	(1)(2)
Natural deformation mode $u = l - l_0$ $\theta_s = \theta_2 - \theta_1$ $\theta_a = \theta_2 + \theta_1 - 2(\varphi - \varphi_0)$	(6)
Function modules from any angle $\theta_a = \underset{2\pi}{\mathrm{mod}}(\theta_a + \pi) - \pi$	(8)
Self-balancing efforts $\boldsymbol{f}_d = \boldsymbol{K}_d \boldsymbol{u}_d$	(9)(29)
Stress in global coordinates $\boldsymbol{f} = \boldsymbol{R}\boldsymbol{S}\boldsymbol{f}_d$	(11)(13)(14)
Tangent stiffness matrix in global coordinate system $\boldsymbol{K} = \boldsymbol{R}\boldsymbol{K}^e\boldsymbol{R}^T$	(13)(17)(39)

4.1 Cantilever beam under pure bending

This example illustrates the ability of the corotational formulation developed in this work to deal with large rigid solid rotations due to the application of the modulus function defined in Equation (8). It involves an embedded beam subjected to a bending moment applied at its free end. As the value of the applied bending moment increases, the beam will roll into circles of progressively smaller radii.

The first circle is formed when $l = 2\pi r$, that is, when one revolution is completed. Thus, the radius of curvature is $r = l/2\pi$, the curvature is $\kappa = 2\pi/l$ and the bending moment is $M = 2\pi EI/l$. Figure 7a details the mechanical and geometrical properties of the beam, which was discretized into 10, 20 and 40 unified beam elements. More refined meshes were used to better represent the circles of smaller radii. A rotation of $2\pi/10$ was imposed on the free end of the beam. Therefore, 10 load steps were necessary to complete one turn. In this example, 8 laps were simulated with 80 load steps, and after 8 laps, the radius assumes the value of $1000/16\pi = 19.89$. It is important to note that after 8 turns, the free end of the beam undergoes a rigid solid rotation at the value of 2880^o. The deformation of the beam shown in Figure 7b was obtained using 40 elements, and it can be observed in this figure that the beam completes 5 turns resulting in the formation of 5 circles. It was not possible to accurately represent 8 circles with the 40-element mesh, because the length of each element is 1000/40 = 25 > 19.89. Therefore, to represent 8 circles, a discretization above 50 elements is necessary. Figure 7c shows the horizontal and vertical displacements of the free end of the beam for 8 laps with the different meshes used. It can be noticed that as the mesh is refined, the better the representation of the magnitude of these displacements with increasing number of rotations. For the discretization with 10 elements, the equilibrium trajectory was obtained with an average number of iterations of 5.68, while with 20 elements this value was 5.04 and with 40 elements the value found was 6.

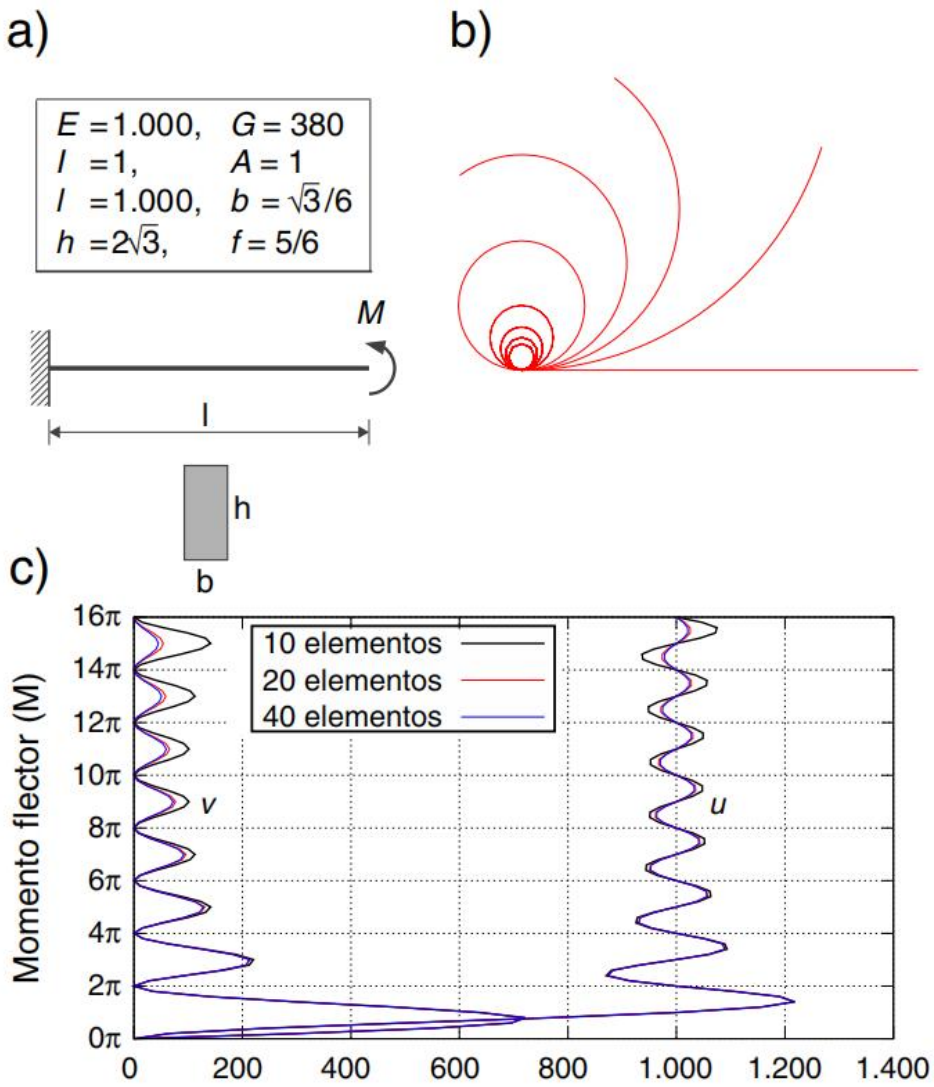

Figure 7. Cantilever beam subjected to pure bending. a) Geometric and mechanical properties. b) Deformation. c) Equilibrium trajectories.

4.2 William's toggle beam

This example consists of two stiffly connected inclined flat beams with embedded ends, subjected to a concentrated load P at the apex. Figure 8a details the geometric and mechanical properties of these beams. Each beam has been discretized with 10 unified beam elements. Figure 8b shows two equilibrium trajectories where the vertical displacement of the apex was monitored for two boundary conditions. The first condition refers to the ends of both embedded beams, while for the second condition supports with two restraints were considered. These results were compared with those obtained by Chan and Chui [15], where a good agreement can be observed. To obtain the equilibrium trajectories for both boundary conditions, the vertical component of the vertex displacement was controlled with the value of -0.025 for 30 load steps. The average number of iterations for the embedded-embedded boundary condition was 2.93 while for the other case it was 3.1. It can be noted that the equilibrium trajectories shown in Figure 8b for both boundary conditions present two limit points.

4.3 Bi-articulated lowered circular arch

In this example, a recessed arch with a circular directrix and both ends supported is considered, which is subjected to a concentrated load P with an eccentricity of 0.2 m relative to its apex.Thus, the load P and a bending moment M = 0.2P applied at the vertex of the arch were considered. Figure 9a details the geometric and mechanical properties of the arch that was discretized with 20 unified beam elements. Figure 9b shows the load curve P versus the vertical displacement υ of the apex. Figure 9c shows the load curve P versus the horizontal displacement u of the vertex. The results of both equilibrium trajectories were compared with those obtained by Chan and Chui [15], where a good agreement can be observed, except, small discrepancies in the size of the loops in relation to the abscissa axis presented in Figure 9c. These discrepancies are probably due to the fact that these points were obtained after digitizing the graphs and adjusting the scales of the coordinate axes. To obtain the equilibrium trajectories, the variable displacement control method presented in reference [16] was used. The value of the arc length was 0.0085 for 315 load steps. The average number of iterations was 3.6. It can be noted that the equilibrium trajectories of the arc shown in Figures 9b and 9c are strongly nonlinear with the presence of some limit points, turning points and loops.

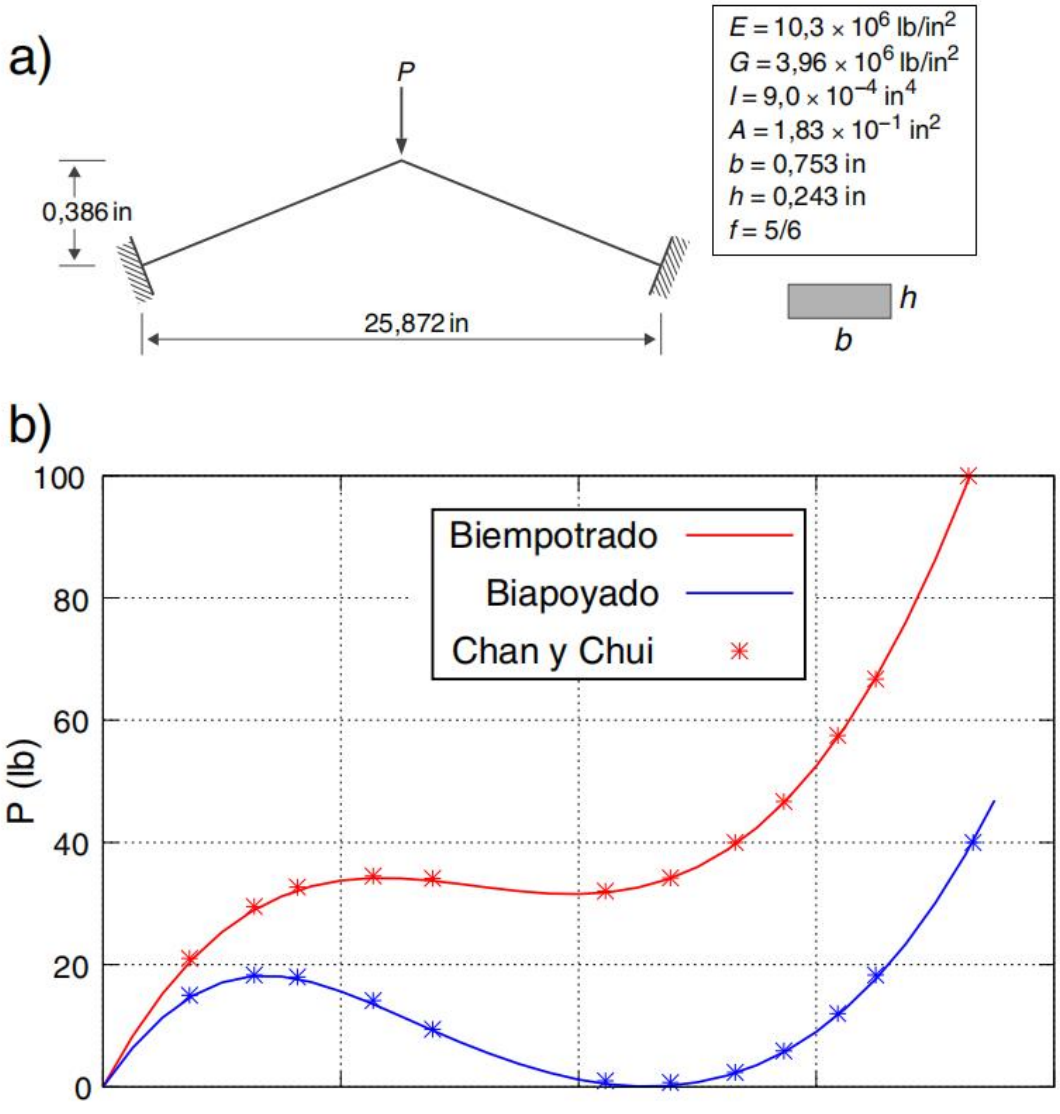

Figure 8. William's toggle beam. a) Geometric and mechanical properties. b) Equilibrium trajectories.

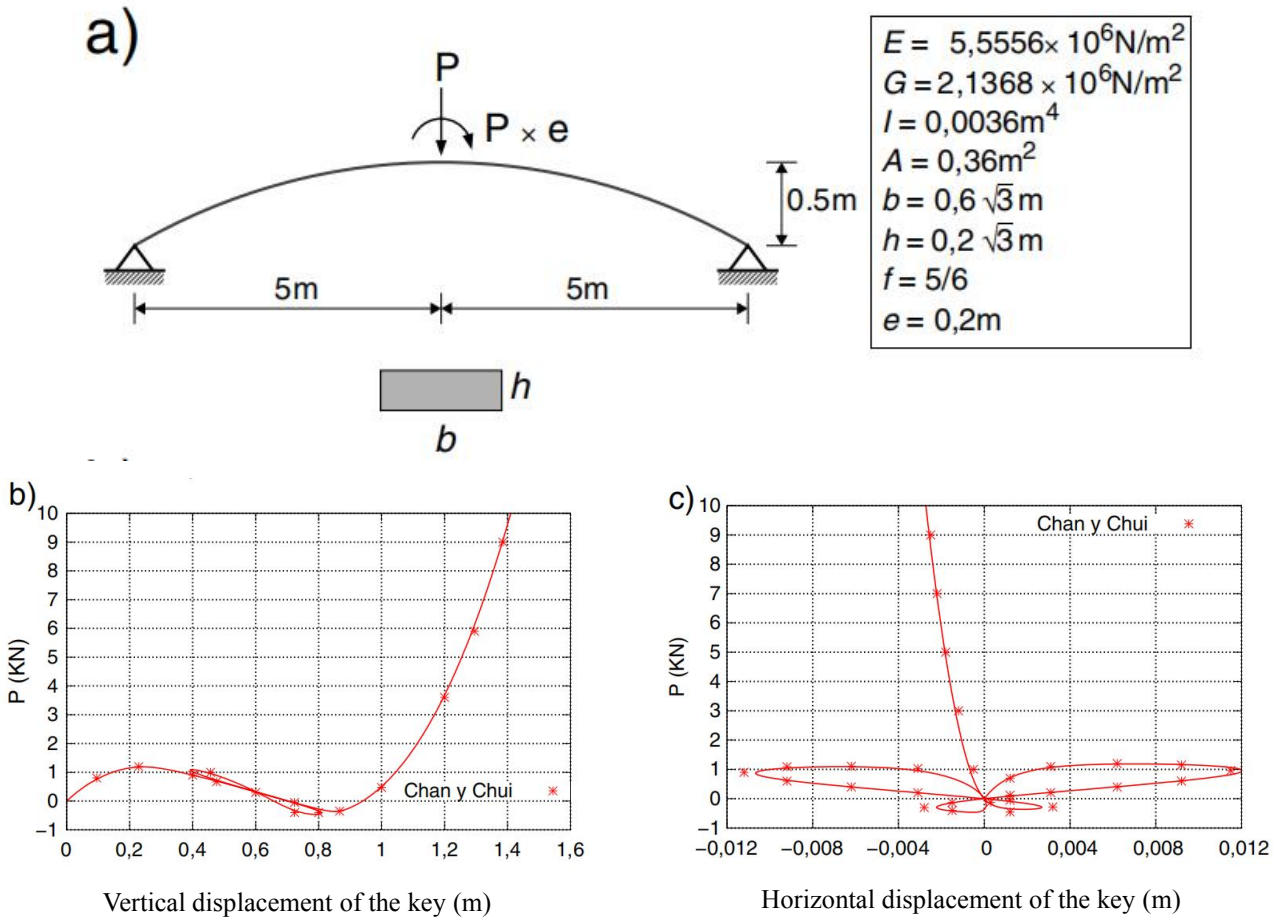

Figure 9. Bi-articulated circular arc with lowered arch. a) Geometric and mechanical properties. b) Vertical displacement of the vertex. c) Horizontal displacement of the vertex.

4.4 Lee's portal frame

This example consists of the connection of a beam and a column, forming a right angle between them. One end has a support with two restraints, while the other end has a support with a restraint allowing displacement in the y-axis direction. The loading conditions as well as the geometrical and mechanical properties are described in Figure 10a. This portal frame was discretized with 10 unified beam elements. Figure 10b shows the equilibrium trajectories, describing the evolution of the vertical displacements v_1 of the rigid node of the portal frame and v_2 of the support of a restraint during the loading process. The results of both equilibrium trajectories were compared with those obtained by Fuji et al. [17] and a good agreement was observed. To obtain the nonlinear response of Lee's gantry, the arc length method with cylindrical constraint was used. The arc length used was 15.1 for 200 load steps. There were 42 automatic cuts due to the divergence of the iterative process. The average number of iterations was 4.52. It can be noted that the equilibrium trajectories of the Lee Gantry, shown in Figure 10b, are also strongly nonlinear with the presence of some limit points, turning points and loops.

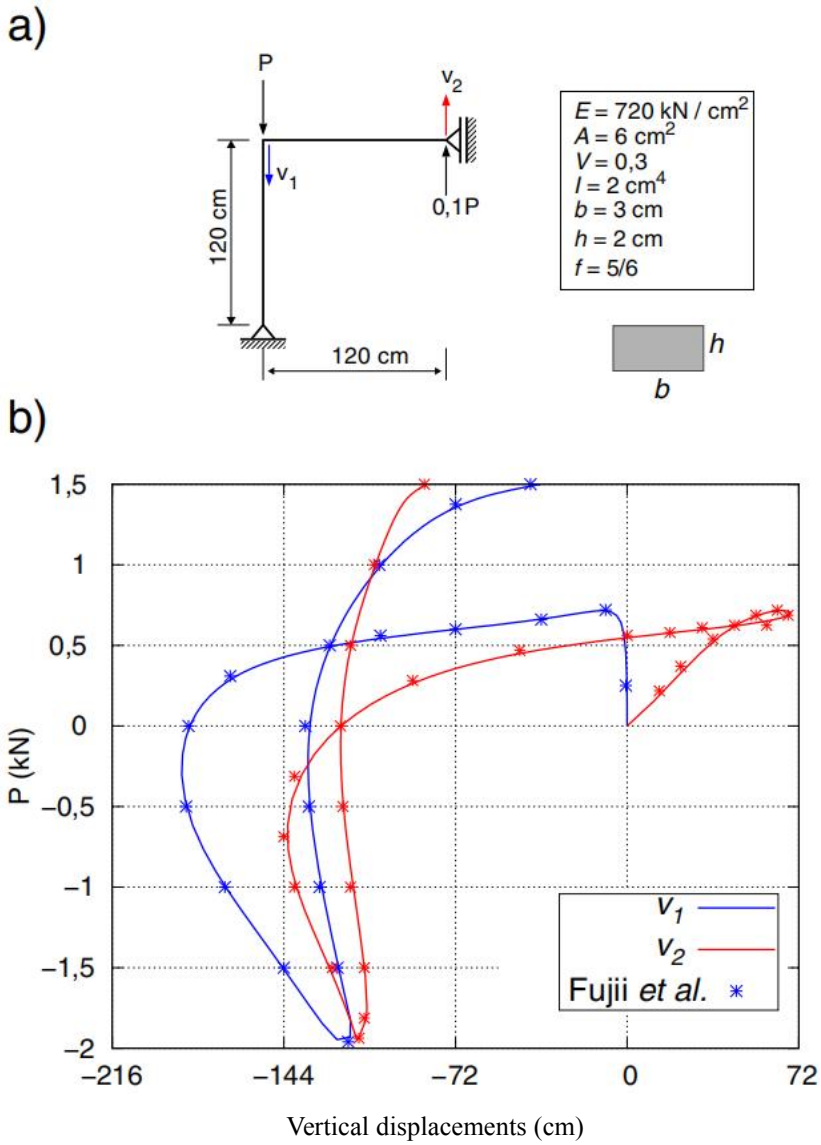

Figure 10. Lee's gantry. a) Geometric and mechanical properties. b) Equilibrium trajectories.

5. Conclusions

In this work, it was shown that, through numerical examples, the ability of the unified beam finite element to deal with large rigid body rotations. This element integrates the Euler-Bernoulli and Timoshenko theories and does not present blocking by shear deformation. Therefore, it does not produce an artificial overstiffness in the nonlinear behavior of different structural typologies. The relationship between the corotational formulation and the natural deformation modes has been described in detail. The great advantage of using the natural deformation modes is that they define a priori the self-equilibrated internal forces, which leads to obtaining the nodal force vector and the consistent tangent stiffness matrix, described in global coordinates through quite simple algebraic operations. On the other hand, the rigid solid motion of the unified beam element and the obtaining of the corotational stiffness matrix have been explicitly described in this work. The main advantage of the corotational formulation is the decoupling between local and global effects, which allows the use of a library of finite elements from linear analysis. The extension of these to geometric nonlinear analysis is given by taking into account the global effects due to rigid solid motion. On the other hand, different physical nonlinearities can be easily incorporated into the corotational formulation because they are local effects.

Conflicts of Interest

The author declares no conflicts of interest regarding the publication of this paper.

References

[1] B. Skallerud, K. Holthe, B. Haugen. 2006. Thin shell and surface crack elements for simulation of combined failure modes. *Computer Methods in Applied Mechanics and Engineering*, 194(21): 2619-2640.

[2] L.L. Yaw, N. Sukumar, S.K. Kunnath. 2009. Mesh free co-rotational formulation for two-dimensional continua. *International Journal for Numerical Methods in Engineering*, 79 (8): 979-1003.

[3] C.A. Felippa, B. Haugen. 2005. A unified formulation of small-strain corotational finite elements: I. Theory. *Computer Methods in Applied Mechanics and Engineering*, 81: 131-150.

[4] M. Mostafa, M.V. Sivaselvan, C.A. Felippa. 2013. A solid-shell corotational element based on ANDES, ANS and EAS for geometrically nonlinear structural analysis. *International Journal for Numerical Methods in Engineering*, 95: 145-180.

[5] W.T. Matias e, L.M. Bezerra. 2009. Uma abordagem unificada da formulacao corotacional para elementos de trelica 2D, trelica 3D e viga 2D. *Revista Internacional de Métodos Numéricos para Cálculo y Diseno en Ingeniería*, 25(2): 163-190.

[6] T.N. Le, J.M. Battini, M. Hjiaj. 2011. Efficient formulation for dynamics of corotational 2D beams. *Computational Mechanics*, 48(2): 153-161.

[7] T.N. Le, J.M. Battini, M. Hjiaj. 2014. A consistent 3D corotational beam element for nonlinear dynamic analysis of flexible structures. *Computer Methods in Applied Mechanics and Engineering,* 269: 538-565.

[8] J. Argyris, H. Balmer, J.St. Doltsinis, et al. 1979. Finite element method - the natural approach. *Computer Methods in Applied Mechanics and Engineering*, 17/18: 1-106.

[9] J. Argyris, H.O. Hilpert, G.A. Malejannakis, D.W. Scharpf. 1979. On the geometrical stiffness of a beam in space - A consistent V.W. approach. *Computer Methods in Applied Mechanics and Engineering*, 20: 105-131.

[10] S. Krenk. 1994. A general format for curved and nonhomogeneous beam elements. *Computers & Structures*, 50: 449-454.

[11] S. Krenk. 2009. *Non-Linear Modeling and Analysis of Solids and Structures*, Cambridge University Press.

[12] M.J. Turner, R.W. Clough, H.C. Martin, L.J. Topp. 1956. Stiffness and deflection analysis of complex structures. *Journal of the Aeronautical Sciences*, 23: 805-824.

[13] J.S. Przemieniecki. 1968. *Theory of Matrix Structural Analysis*, McGraw-Hill.

[14] H.C. Martin. 1966. On the derivation of stiffness matrices for the analysis of large deflection and stability problems, AFFDL-TR-66-80. *Air Force Institute of Technology*, pp. 697-716.

[15] S.L. Chan, P.P.T. Chui. 2000. Non-linear static and cyclic analysis of steel frames with semi-rigid connections, Elsevier, Amsterdan.

[16] W.T. Matias. 2002. El control variable de los desplazamientos en el análisis no linealelástico de estructuras de barras. *Revista Internacional de Métodos Numéricospara Cálculo y Diseno en Ingeniería*, 18(4): 549-572.

[17] F. Fujii, K.K. Choong, S.X. Gong. 1992. Variable displacement control to overcome turnning points of nonlinear elastic frames. *Computers & Structures*, 44(1/2): 133-136.